ERDA/NASA 1011/77/1
NASA TM X-73629

ELECTRIC VEHICLE POWER TRAIN INSTRUMENTATION - SOME CONSTRAINTS AND CONSIDERATIONS

James E. Triner and Irving G. Hansen
National Aeronautics and Space Administration
Lewis Research Center
Cleveland, Ohio 44135

Work performed for
ENERGY RESEARCH AND DEVELOPMENT ADMINISTRATION
Office of the Assistant Administrator for Conservation
Division of Transportation Energy Conservation
Under Interagency Agreement EC-77-A-31-1011

Technical Paper to be presented at International Electric Vehicle Exposition sponsored by the Electric Vehicle Council Chicago, Illinois, April 26-29, 1977

ELECTRIC VEHICLE POWER TRAIN INSTRUMENTATION - SOME CONSTRAINTS AND CONSIDERATIONS

by James E. Triner and Irving G. Hansen

National Aeronautics and Space Administration
Lewis Research Center
Cleveland, Ohio 44135

E-9125

ABSTRACT

The application of pulse modulation control (choppers) to DC motors creates unique instrumentation problems. In particular, the high harmonic components contained in the current waveforms require frequency response accommodations not normally considered in DC instrumentation.

In addition to current sensing, accurate power measurement requires not only adequate frequency response but must also address phase errors caused by the finite bandwidths and component characteristics involved.

This paper will discuss the implications of these problems, and report on the degree to which they have been solved at Lewis Research Center.

INTRODUCTION

The DC series type motor has been used for many years for traction type applications because it has desirable speed torque characteristics. In early vehicles, power losses incurred with dissipative type regulators were accepted as the penalty resulting from achieving the desired level of control. With the development of high power semiconductor switches [Ref. 1], the application of pulse width modulation techniques ("chopping") substantially reduced the power system losses.

STAR category 33

Pulse width modulation (PWM) controls the average voltage applied to the motor by controlling the on time of the switch. The resulting average current is controlled, but at the expense of high peak current drawn from the source or, high crest factor operation [Ref. 2].

The effects of PWM on the power system performance are the subjects of other investigators [Refs. 3 and 4]. This paper documents measurement errors resulting from the high crest factor current pulses of PWM and recommends instrumentation techniques to achieve the accuracies specified in SAE XJ227(A) "electric vehicle test procedure" [Ref. 5] paragraph 3.4 which allows a maximum of ±2% full scale error.

To understand the measurement errors incurred in the control and instrumentation of PWM controlled power systems it is necessary to define the dynamic (AC) characteristics as well as the static (DC) characteristics of the power train and the instrumentation sensors.

The DC characteristics are easily understood, and are sometimes regarded as the only input during system modeling and analysis. This is misleading since the AC characteristics hold the key to understanding the inherent nonlinear characteristics of the total system. Questions such as overall efficiency, system performance, input and output loading characteristics, and system response can only be answered by accurate static/dynamic DC/AC wideband modeling and analysis of the physical subsystem components.

Dynamic Characteristics

A simplified schematic for a DC/DC chopper is shown in Fig. 1(a). For convenience, the series motor is assumed to be operating in a stable manner with its armature current (Im) varying between Imax and Imin. When Im is equal to Imin the switch is closed and Im begins to increase towards Imax (Fig. 1(b)).

When the armature current reaches Imax the switch opens, and the energy stored in the series field maintains the armature current through the free wheeling diode. During this portion of the circle the terminal

voltage of the motor is limited to the low forward drop of the free wheeling diode (Fig. 1(c)).

This is the text book idealized description of chopper operation. It is presented only to provide a foundation for the observations to follow:

(a) The current Ib flows from the source only during the time that the switch is closed. It is to be noted that the rise and fall times of this current are limited only by the external circuit parameters, not by the motor inductance. In addition, brush shorting times, system storage, and various stray effects all add high frequency components that must be measured in order to define the actual input current. A typical input current would look much like Fig. 1(d). Due to battery droop and IR drops the voltage across the chopper input appears as shown in Fig. 1(e).

(b) In addition to the case illustrated, in practice some choppers interrupt the negative line to the motor. Such a system may have the negative line connected to instrument ground, either by design or accidently by virtue of degraded isolation. It is to be observed that this alternate connection will present the instrument system with a common mode voltage at least equal to the system supply voltage. This problem must be addressed in the design of any instrument monitoring such a chopper system.

Instrumentation of a Chopper System

The two sets of fundamental parameters that are readily available to analyze the chopper system are (1) input voltage and current, and (2) output voltage and current. Present technology for wideband voltage measurements present little problem in achieving accurate input/output voltage measurements.

However, the instrumentation for accurate wideband current measurements are not as readily available. DC sensor limitations such as range, AC response, and nonlinear transfer characteristics, can often lead to erroneous data. The results of utilizing this inaccurate data are incorrect efficiencies, unexplainable system performance, unpredictable input/output loading characteristics, and unreliable system response.

Model of a Wideband Current Sensor

To aid in assessing the present state-of-the-art of wideband high current measurements, an analysis will be shown for the equivalent circuit of a high current sensor to determine the appropriate transfer functions. The model can be reduced to a simple resistor R_{DC} for the DC case, but is a complex function of frequency under AC conditions. As shown below, the model consists of a series-parallel network consisting of inductance L, resistive elements R_{DC}, which is independent of frequency, and R_{AC}, which is a function of frequency due to skin effect, and capacitance C.

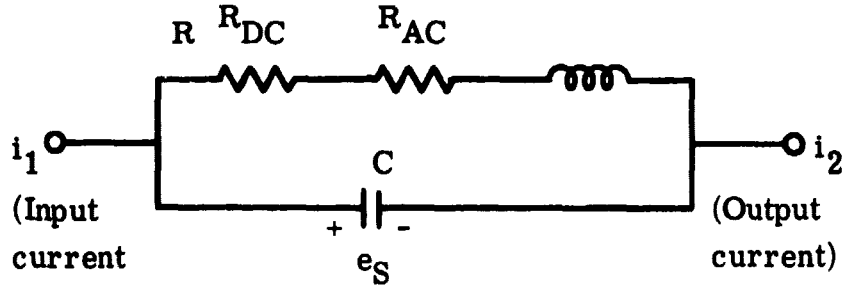

The following wideband properties can be derived for the above model:

$$Z = \frac{R_{DC} + R_{AC} + J\omega\ L(1 - \omega^2\ LC) - C(R_{AC} + R_{DC})^2}{(1 - \omega^2\ LC)^2 + \omega^2 C^2 (R_{DC} + R_{AC})^2} \tag{1}$$

$$|Z| = \left| \frac{(R_{DC} + R_{AC})^2 + \omega^2 L^2}{(1 - \omega^2\ LC)^2 + \omega^2 C^2 (R_{DC} + R_{AC})^2} \right|^{1/2} \tag{2}$$

$$\text{phase angle } \varphi = \tan^{-1} \frac{\omega \left[L(1 - \omega^2 LC) - C(R_{DC} + R_{AC})^2 \right]}{R_{DC} + R_{AC}} \tag{3}$$

and

$$\frac{e_s}{i_1} = Z_s = \text{current sensor transfer impedance} \tag{4}$$

Note that as the frequency approaches zero, i.e., $\omega \to 0$, the complex DC/AC model reduces to

$$Z = \frac{R_{DC}}{(1)^2} = R_{DC} \tag{5}$$

$$|Z| = \left[\frac{(R_{DC})^2}{(1)^2} \right]^{1/2} = R_{DC} \tag{6}$$

$$\text{Phase angle } \varphi = \tan^{-1} \frac{0}{R_{DC}} = 0 \tag{7}$$

$$\frac{E_S}{I_1} = R_{DC} \tag{8}$$

Subsequently, voltage, current, and power relations can be represented simply by applying Ohm's law:

$$E_S = I_I R_{DC} \qquad I_1 = \frac{E_S}{R_{DC}} \qquad P_S = I_1^2 R_{DC} = \frac{E_S^2}{R_{DC}}$$

However, to apply these same equations for AC system parameters it is clear that substantial error would be incurred due to frequency dependent magnitude changes, and compounded further for power measurements due to frequency dependent phase angle changes. In addition to the above frequency dependent changes due to L and C, the effective AC resistance (R_{AC}) of the model is also dependent on frequency due to skin effect. The skin depth and the resistance per square in rationalized units, are [Ref. 4]:

$$\delta = \left(\frac{\lambda}{\pi\sigma\mu C}\right)^{1/2} \text{M}$$

$$R_{SQ} = \frac{1}{\delta\sigma} \Omega$$

where

$$C = 2.998\times10^{8} \frac{\text{M}}{\text{S}}$$

$$\mu = 4\pi\times10^{-7} \mu_r \frac{\text{H}}{\text{M}}$$

$$\frac{1}{\sigma} = 1.724\times10^{-8} \frac{\rho}{\rho_c} \Omega - \text{M}$$

From these equations, the R_{AC} term can be calculated for different types of current probe configurations. For a rectangular configuration the resistance/foot would be:

$$R_{AC} = \frac{12}{AB} R_{SQ}$$

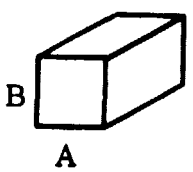

and, for a cylindrical configuration:

$$R_{AC} = \frac{12}{\pi D} R_{SQ}$$

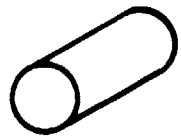

To make a comparison of commercially available wideband current sensors, a study must be made of the magnitude and phase angle transfer characteristics versus frequency. From these data one can determine the major parameters such as frequency response, bandwidth, range, and percent error for both current magnitude and power measurements.

RESULTS AND DISCUSSION

Comparison of Wideband Current Sensors

To determine the state-of-the-art of commercially available wideband current sensors, four types were investigated and analyzed to determine their applicability to the measurement of key electric vehicle power train currents. The four types are the: (1) standard DC current shunt (e.g., 200 mV at 500 A), (2) narrowband clamp on DC current sensor (0 to 600 A range), (3) co-axial resistor current sensor, and (4) wideband Hall effect current sensor.

The transfer characteristics of each of these sensors were measured and are shown in Figs. 2 and 3. To analyze each of the sensor characteristics, the equivalent model discussed earlier will be applied.

Standard DC current shunt - Equation (2) is used to determine the accuracy of the shunt for current measurements only. For a typical standard shunt, $C << 1\mu F$, $L < 1\mu H$, $R_{DC} < 10\ m\Omega$, and $R_{AC} = k\sqrt{f}$ $(0 < R_{AC} > R_{DC})$. For these characteristic values, $\omega^2 LC << 1$ and $\omega^2 C^2 (R_{DC} + R_{AC})^2 << 1$, the magnitude equation is reduced to:

$$|Z| = \left[(R_{DC} + R_{AC})^2 + \omega^2 L^2 \right]^{1/2}$$

Plotting $|Z|$ versus f with $R_{DC} = 0.0063\Omega$, $L = 0.2\mu H$, and $R_{AC} = k\sqrt{f}$ yields the plot shown in Fig. 2(a). There is good correlation between the theoretical and measured impedance of the current sensor. The major nonlinearity in the magnitude of the probe is due largely to skin effect (R_{AC}). The useful bandwidth of this sensor for a 1% current error is 2 kHz. If this sensor were to be used for power measurements, the effect of the phase angle is shown by eq. (3). If $W^2 LC \ll 1$ and $C(R_{DC} + R_{AC})^2 \ll L$ the phase angle equation is reduced to

$$\varphi = \tan^{-1} \frac{WL}{R_{DC} + R_{AC}}$$

Plotting φ versus f with the same values for L, R_{AC}, and R_{DC} yields the plot shown in Fig. 2(a). There is a good correlation between the theoretical and measured phase angle φ of the sensor. For power measurements, the useful bandwidth for 1% error is 1 kHz.

Narrow band clamp on current sensor - The high frequency characteristics of this sensor are deteriorated by the same effects as that of the conventional sensor. However, the output of the basic current sensor is compensated using an operational amplifier. Figure 2(b) shows the frequency response of the sensor and compensated amplifier. The probe bandwidth is 1.3 kHz for a 1% error. The phase angle transfer characteristics of the amplifier and the effects of the sensor itself can be seen in the φ versus f plot (Fig. 2(b)) of the current sensor. For power measurements the useful bandwidth for 1% error is 225 Hz.

If this type of current sensor were applied to attain control information from the electric vehicle power train, close attention would have to be paid to maintain overall system stability due to the slim phase margin that this type of sensor would provide.

Co-axial resistor current sensor - The transfer characteristics of this type of current sensor (Fig. 3(a)) are almost identical to the DC case of the current sensor model (eqs. 5-8). Both the magnitude and phase angle are essentially independent of frequency up to 40 MHz (manufacturer's data).

This result is consistent with the typical co-axial transmission line parameters where:

$$C = \frac{2\pi\epsilon}{\ln\left(\frac{b}{a}\right)} \frac{F}{M} \qquad \text{capacitance/unit length}$$

$$C_7 = \frac{2\pi\sigma}{\ln\left(\frac{b}{a}\right)} \frac{\Omega^{-1}}{M} \qquad \text{conductance/unit length}$$

$$L_{EXT} = \frac{\mu}{2\pi} \ln\frac{b}{a} \frac{H}{M} \qquad \text{inductance/unit length}$$

L_{EXT} is an external inductance and does not take into account any flux within either conductor. At typical operating frequencies (<40 MHz) the skin depth is so small that there is negligible flux within either conductor and negligible interior inductance. These characteristics indicate that this type of current sensor could be used as a standard for both analyzing electric vehicle performance and calibration of other types of instrumentation. The accuracy of this sensor for both current and power measurements can be $<<$ 1% for bandwidths up to 40 MHz.

Wideband Hall effect current sensor - From Fig. 2(b), it is clear that the transfer characteristics of this sensor are almost identical to that of the co-axial current sensor except for usable bandwidth. For current and power measurements the useful bandwidth for <1% error is >20 kHz.

Fourier Analysis

For electric vehicle power trains employing some form of pulse width modulation control, the ideal current waveforms can be represented as a ratio of the on-time to the total period $T(T_{ON} + T_{OFF})$ as follows:

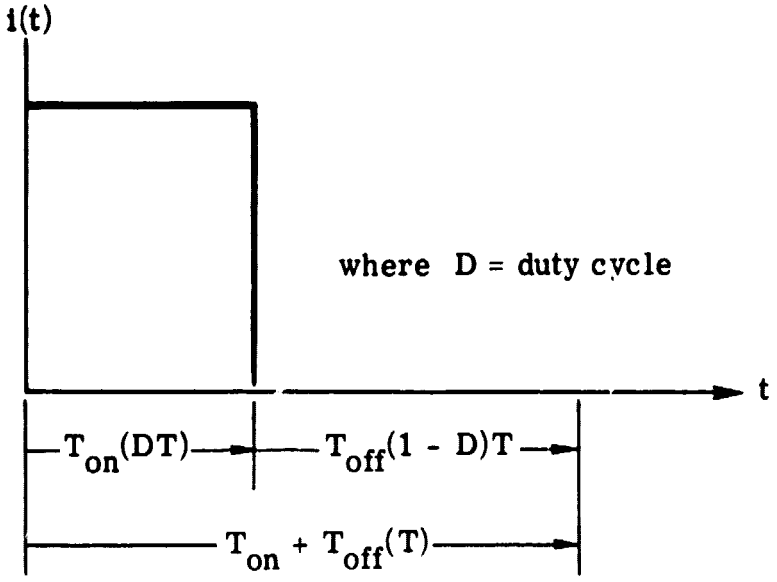

Since these pulse are continuous with time they have a characteristic for a constant load which appears as follows:

By proper selection of time scale t, the input current pulses become even functions of time:

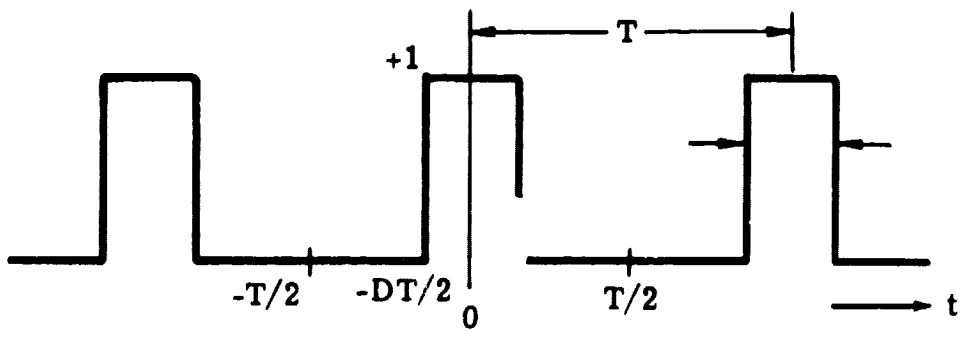

The Fourier series of this PWM pulse train can be shown to have a similar spectrum to that of the Fourier integral of a single pulse [Ref. 6]. This similarity is shown below:

Fourier series

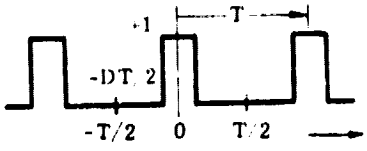

$$A_n = \frac{1}{T}\int_{-DT/2}^{DT/2} e^{-jnt}\,dt$$

$$f(t) = \sum_{n=-\infty}^{\infty} \frac{D \sin \frac{n\Omega T}{2}}{\frac{nDT}{2}}$$

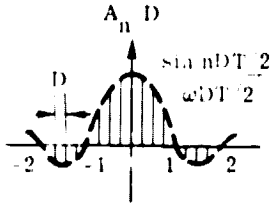

(Line spectrum)

Fourier integral

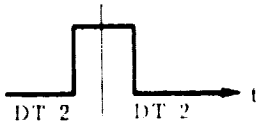

$$g(W) = \frac{1}{T}\int_{-DT/2}^{DT/2} e^{-j\omega t}\,dt$$

$$f(t) = \int_{-\infty}^{\infty} \frac{D \sin \omega \frac{DT}{2}}{\omega \frac{DT}{2}} e^{j\omega t}\,d\omega$$

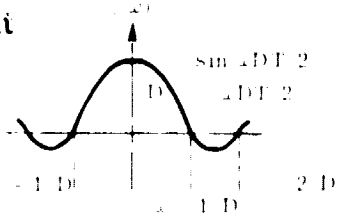

(Continuous spectrum)

Effect of bandwidth limitations - As shown in the previous section, the inverse Fourier transform for the rectangular pulse is:

$$f(t) = \int_{-\infty}^{\infty} \frac{D \sin \omega \frac{DT}{2}}{\omega \frac{DT}{2}} e^{j\omega t} \, d\omega$$

Since the bandwidth of the measurement equipment is generally limited, the limits of integration are restricted to $\omega_0 << \infty$ thus,

$$f(t) = \int_{-\omega_0}^{\omega_0} D \frac{\sin \omega \frac{DT}{2}}{W \frac{DT}{2}} e^{j\omega t} \, d\omega$$

For typical electric vehicles applications the range of values for T and D are:

$$0.002 < T < 0.01 \text{ sec}$$

$$0.01 < D < 1$$

For $T = 0.006$ sec and $D = 0.1$ a quick inspection indicates that a bandwidth of 3.33 kHz might be adequate to reproduce this pulse accurately. However, this conclusion might be inaccurate unless supported by analysis of the frequency spectrum. If the inverse Fourier integral were evaluated for $\omega_0 = 2\pi \cdot 3.3 \times 10^3$ the following result is obtained:

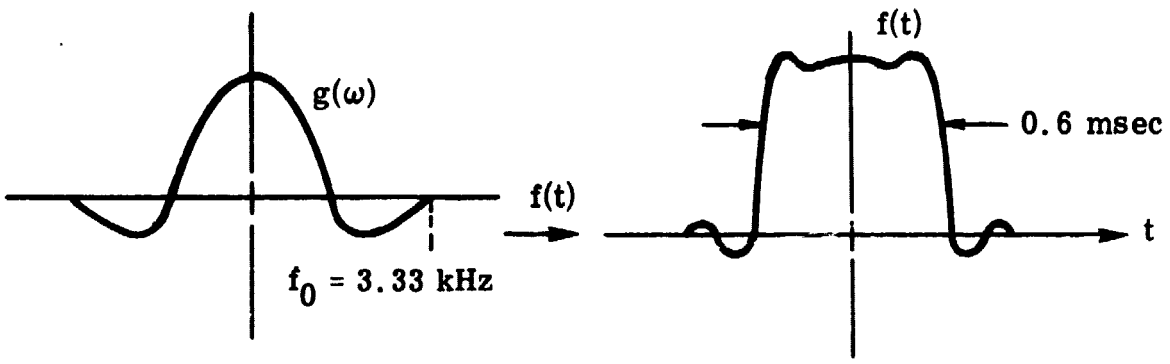

Therefore, a pulse similar to the original pulse, with the exception of slight rounding of the corners, is transmitted. However, if D = 0.01 the corresponding frequency response would have to be 33.3 kHz. Since, the equipment would have a limited bandwidth of 3.33 kHz the effect on the pulse transmitted would be:

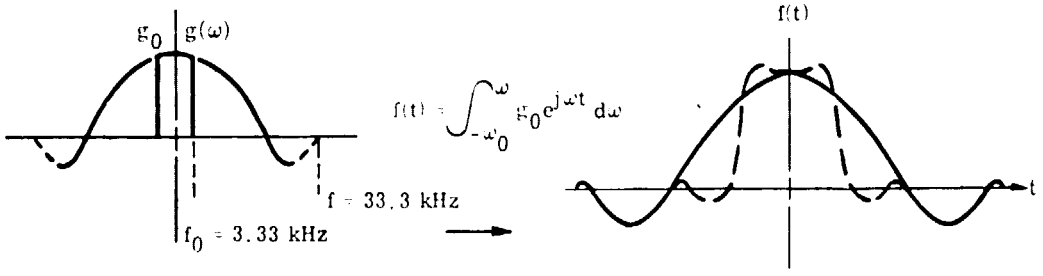

Thus, the rectangular pulse has degenerated as a result of limited bandwidth.

Similar results were reported by J. B. Folsom for the measurement of "true-rms" signals [Ref. 7]. The error is plotted as a function of bandwidth/fundamental frequency and crest factor. Crest factor is defined as the ratio of the peak value to the rms value of the waveform. Similar

results to those obtained by the inverse Fourier transform with limited bandwidth are shown in Fig. 4 (i.e., as $DT \rightarrow 0$ bandwidth $\rightarrow \infty$ for % error = constant).

This is an important result to take into account especially for measuring the true characteristics of electric vehicle power trains operating under PWM conditions. The instrumentation bandwidth must be adequate to insure accurate data acquisition over the entire operating range of the power train controller.

Based on the above investigations the co-axial type resistor will be used as the Lewis Research Center standard in the checking and calibration of other current sensors. Calibration of current sensors will comprise both pulse calibration and gain and phase measurement as a function of frequency.

Power Measurements

Figure 5 is a photograph of the terminal voltage measured on an EV-106 traction battery under pulse discharging. Note that the battery voltage, which is often times taken at its average value for power calculations, significantly droops during the "on time." Or stated in another way the actual power delivered is less than would be indicated by an average voltage measurement.

The actual power drawn from the battery is the instantaneous product of the voltage and current.

Compliance with the electric vehicle test procedure SAE XJ227(A) [Ref. 5] requires a measurement error of less than ±2%. At first glance a power measurement having this accuracy does not appear to be too difficult to implement. However, many phenomena are involved, any one of which may easily cause errors well in excess of the allowance. Some of the more obvious of these are:

(1) Envelope distortion: This is directly analogous to the phase shift encountered in conventional single frequency AC circuitry, and indeed is caused by phase shifts in the various frequency components involved. Any distortion or delay of the waveforms will result in serious errors. These distortions may be due to limited bandwidths and phase response of the sensors as discussed earlier. Limited bandwidths in signal conditioning associated with either the voltage or current measurement (an area of particular concern is the voltage isolation amplifier), or even quadrature components magnetically induced in signal lines will create significant distortions and phase shifts.

(2) Scale factors in the multiplier: Output offsets, thermal drifts, and transfer linearities are typically specified relative to the full scale product. A traction motor will draw peak armature currents many times larger than its typical constant speed current. The result is a power measurement having a full scale value much larger than the nominal power measured, with a consequent degrading of what would initially appear to be an accurate measurement.

A final observation on bandwidths is in order. While the voltage and current components involved in the power measurement have high frequency components, power by definition is always an average. Therefore, the output of the multiplier may have a relative limited bandwidth with no loss in accuracy.

A laboratory type wideband wattmeter using electronic multipliers has been evaluated at the Lewis Research Center. Power measurements were verified to be accurate within ±0.5% of full scale for all voltage and current components with a bandpass of DC to greater than 20 kHz. This wattmeter has been chosen for electric vehicle service testing and is presently being modified for vehicle service.

CONCLUSIONS

The application of pulse width modulation control (choppers) to DC motors creates unique instrumentation problems. It has been shown that high harmonic components in current waveforms require frequency response accommodations not normally considered in DC instrumentation.

A mathematical equivalent circuit of a current sensor was developed. It was experimentally verified that the model accurately represents the response to higher frequency components. Standard shunts were found to have the greatest error (greater than 2% at a few kHz and greater than 100% at 20 kHz) while the co-axial resistor specified was accurate to within ±0.25% from DC to 40 MHz [Ref. 8]. Based on these results, Lewis Research Center plans to use the co-axial resistor as a calibration standard. Electric vehicle current sensors will be of the wideband Hall effect type, calibrated under pulse conditions against the co-axial standard resistor.

Conventional power measurements utilizing standard current shunts and averaging type meters will result in errors easily an order of magnitude in excess of the ±2% required by the SAE test procedure. The absolute value of error will vary as a function of the pulse repetition rate and duty cycle. Also, errors in power measurements will occur not only from current sensing errors, but also are affected by phase and bandwidth limitations of the voltage measurement, resulting in improper definition of what constitutes the "input power" to the vehicle system.

REFERENCES

1. Dewan, S. B.; and Straughen, A.: Power Semiconductor Circuits. John Wiley and Sons, 1975.

2. Amato, C. J.: Latent Losses in 'Lectric Lizzies. IEEE Trans. Ind. Gen. Appl., vol. IGA-5, no. 5, Sept./Oct. 1969, pp. 558-565.

3. Demerdash, N. A. O.; and Hamilton, H. B.: Effect of Complex Forms on Copper Losses in Large D.C. Motors. IEEE Conference Record of Fifth Annual Meeting of Industry and General Applications Group, Inst. Electr. Electron. Eng., Inc., 1970, pp. 77-81.

4. Reference Data for Radio Engineers. 4th ed., International Telephone and Telegraph Corp., 1956.

5. Electric Vehicle Test Procedure. SAE Recommended Practice XJ 227(A).

6. Skilling, H. H.: Electrical Engineering Circuits. Wiley and Sons, 1965.

7. Folsom, J. B.: That "True-RMS" Meter: Will It Be True to You? EDN, vol. 20, no. 20, Nov. 1975, pp. 91-95.

8. Silsbee, F. B.: Notes on the Design of Four-Terminal Resistance Standards for Alternating Current. Bureau of Standards Journal of Research, Vol. 4, January 1930.

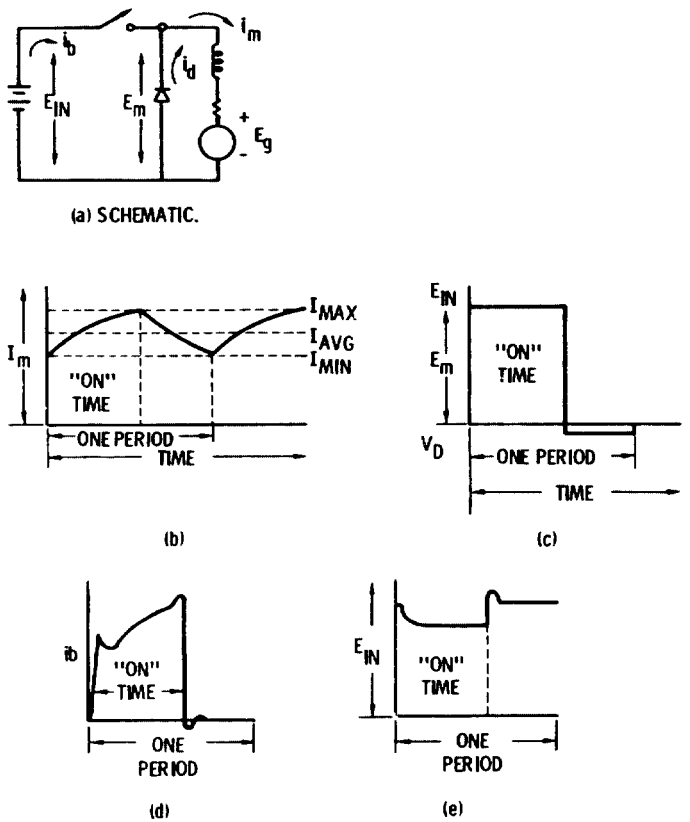

Figure 1. - Typical operating characteristics for a DC/DC chopper.

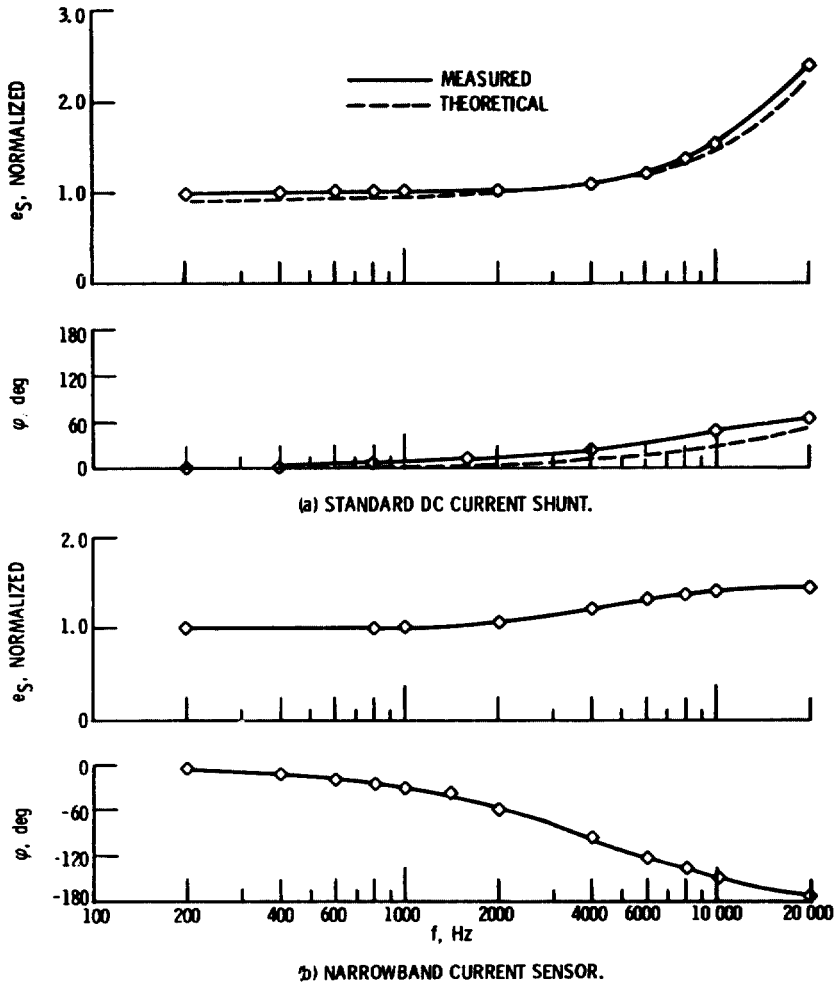

Figure 2. - Gain and phase characteristics of a standard DC current shunt and a narrowband current sensor.

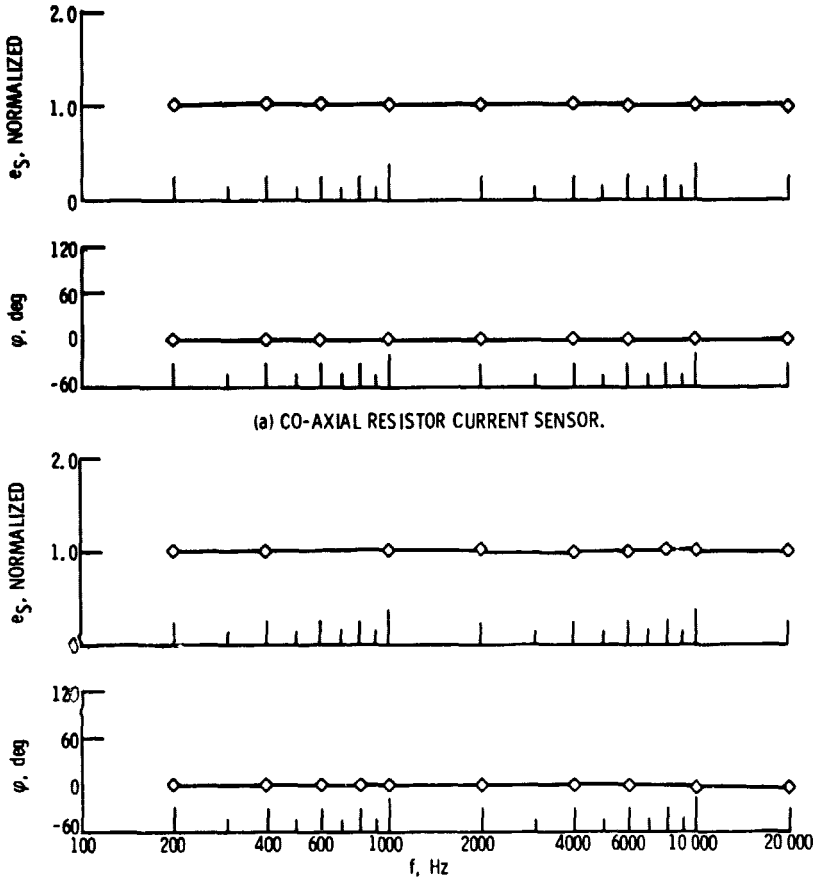

(a) CO-AXIAL RESISTOR CURRENT SENSOR.

(b) WIDEBAND HALL EFFECT CURRENT SENSOR.

Figure 3. - Gain and phase characteristics of a co-axial resistor current sensor and a wideband Hall effect current sensor.

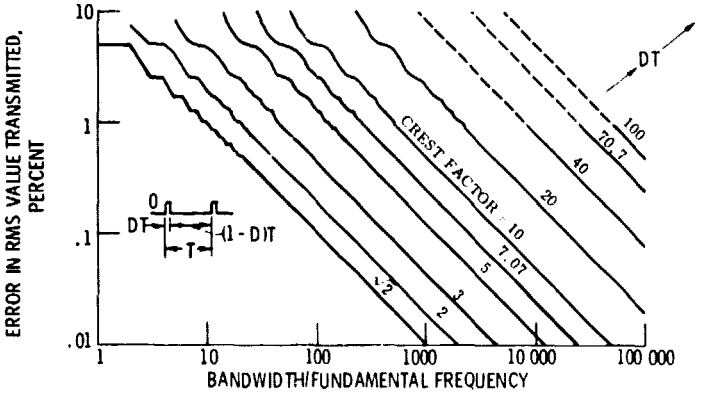

Figure 4. - Error versus crest factor and bandwidth for rectangular pulse trains.

Figure 5. - Battery E/I characteristics.